AUTOMATED SPHERE GEOMETRY OPTIMIZATION FOR THE VOLUME MULTI-SPHERE METHOD

Philip Chow, Joseph Hughes, Trevor Bennett, and Hanspeter Schaub

26th AAS/AIAA Spaceflight Mechanics Meeting

AUTOMATED SPHERE GEOMETRY OPTIMIZATION FOR THE VOLUME MULTI-SPHERE METHOD

Philip Chow[*] **Joseph Hughes**[†] **Trevor Bennett**[‡] **and Hanspeter Schaub**[§]

The Volume Multi Sphere Method (VMSM) is a recent method for approximating the electrostatic forces and torques acting on a spacecraft. VMSM reduces the conducting spacecraft shape to a collection of equipotential spheres spread throughout the spacecraft volume. The location and size of these spheres are dependent on the spacecraft geometry being modeled. Prior work illustrates the existence and prospect of this VMSM approach on a cylinder, but it took considerable hand tuning to arrive at a suitable VMSM solution. This paper investigates the VMSM setup process itself. In particular, a modified VMSM optimization approach is presented which seeks to avoid any time-consuming hand tuning. The symmetric cylinder problem is investigated with a range of VMSM spheres and a new capacitance constraint that significantly reduces computational time with minimal effect on accuracy.

INTRODUCTION

At Geosynchronous Earth Orbits (GEO), spacecraft can be charged to high voltages — in the range of tens of kiloVolts — due to interactions with plasma in space.[1,2] Of importance is the ability to predict how a charged spacecraft will interact with the Earth's magnetic and electric fields as well as other neighboring charged spacecraft. These interactions cause forces and torques to act on the spacecraft, which in turn affect the attitude and orbital dynamics of the spacecraft. A controlled spacecraft near an uncontrolled object can take advantage of these electrostatic forces and torques to remotely influence the object's attitude and orbit.[3]

One concept using electrostatic charging is the space tug called the Geosynchronous Large Debris Reorbiter (GLiDeR), which alters the charge of an uncontrolled spacecraft within the plasma environment at GEO as shown in Figure 1.[4] By altering the charge of the spacecraft, forces and torques can be applied to the spacecraft remotely, allowing for actions such as the safe detumble,[5] disposal of debris at GEO,[6,7] and orbit corrections[3] to be quickly implemented. With electrostatic charging, detumbling an object rotating at 2 degrees per second to near zero rates can be accomplished within 3-7 days depending on the tug size and voltages used,[5] and increasing the perigee of an orbit by 300 kilometers can be done in less than three months.[3] To touchlessly change the dynamics of an uncontrolled object in this manner, it is necessary to be able to model and predict the dynamics of the system faster than real-time.

---

[*] Graduate Research Assistant, Aerospace Engineering Sciences, University of Colorado, Boulder, CO, USA

[†] Graduate Research Assistant, Aerospace Engineering Sciences, University of Colorado, Boulder, CO, USA

[‡] Graduate Research Assistant, Aerospace Engineering Sciences, University of Colorado, Boulder, CO, USA

[§] Alfred T. and Betty E. Look Professor of Engineering, Associate Chair of Graduate Affairs, Department of Aerospace Engineering Sciences, University of Colorado, 431 UCB, Colorado Center for Astrodynamics Research, Boulder, CO 80309-0431. AAS Fellow
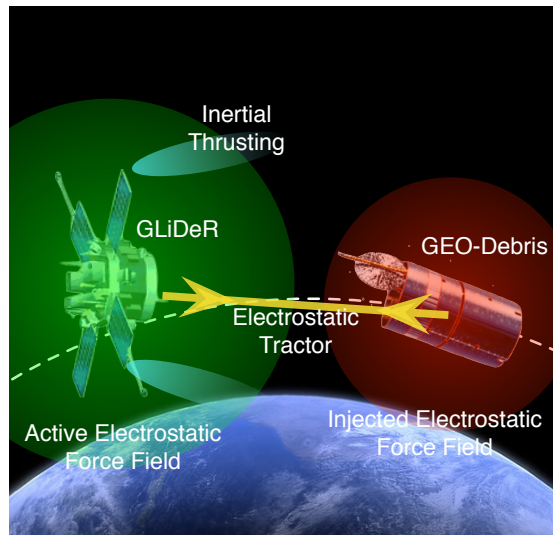
Figure 1. Electrostatic Space Tug Concept Illustration.[7]

Electrostatic charging also offers the potential for propellantless propulsion by harnessing the Lorentz force, which results from the interaction between a charged, moving spacecraft and a planet's electric field. The Lorentz force imparted onto a a spacecraft can be used for station-keeping[8,9] and boosting gravity assist maneuvers.[10] As with the space tug concept, utilizing the Lorentz force in this manner requires the ability to model electrostatic charge distribution on the spacecraft.[11]

All these applications require a methodology to evaluate the spacecraft electrostatic forces and torques in faster-than-realtime numerical simulations. The Multi-Sphere-Method (MSM) is an approach to compute the force and torque with enough fidelity to be believable, but with enough speed to be useful.[11,12] In particular the Volume MSM (VMSM) approach seeks the optimal placement of N spheres within the volume of the spacecraft whereby a small number of spheres to approximate the electrostatic forces and torques on a charged spacecraft. However, as noted in Reference 11, the original setup process in that work to find an optimal VMSM solution can be very challenging and involve some hand tuning of the optimization process. This setup challenge was the key reason for developing the Surface MSM (SMSM) approach. Here the setup process is greatly simplified at the expense of an increased number of spheres. This paper investigates how the VMSM setup can be automated. In particular, the uniqueness of different VMSM solutions to a given set of force and torque truth values is investigated. A range of cost functions are explored to quantify the fit of a given VMSM solution being considered. Different metrics can weight long- or short-range errors differently, and can each be of interest depending on the spacecraft mission scenario.

MULTI-SPHERE METHOD OVERVIEW

One way to calculate the electrostatic forces and torques on a spacecraft is to use a commercial FEA tool, such as ANSYS's Maxwell 3D. However, even with relatively low accuracies, these tools usually require on the order of minutes to complete analyses of simple two-body systems, which is unsuitable for modeling dynamics in real-time for state estimation or control applications.

By reducing the spacecraft geometry to a collection of charged spheres, the configuration of
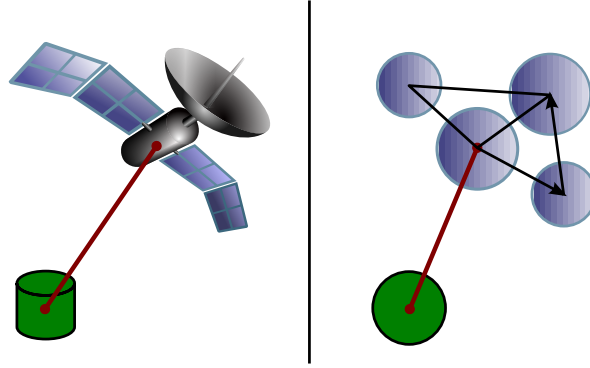
Figure 2. Approximation of a satellite as a collection of charged spheres.[11]

which are dependent on the geometry and conductivity of the spacecraft being modeled, MSM can approximate electrostatic forces and torques several orders of magnitude more quickly than commercial FEA tools with minimal decrease in the resulting accuracy.

As shown in Figure 2, MSM approximates a spacecraft as a collection of spheres with variable positions and radii. The voltage on any sphere is a function of both its own charge and the charge of nearby spheres. If these spheres are far enough away to be approximated as point charges, the voltage is given by:[11]

$$V_i = \frac{1}{4\pi\epsilon_0}\frac{q_i}{R_i} + \sum_{j=1,\,j\neq i}^{m}\frac{1}{4\pi\epsilon_0}\frac{q_j}{\rho_{i,j}} \tag{1}$$

Where q_i and R_i are the charge and radius of the ith sphere, respectively, $\rho_{i,j}$ is the center-to-center distance between spheres i and j, and ϵ_0 is the permittivity of free space constant. If the voltages of each sphere are given by $\boldsymbol{V} = [V_1, V_2, ...V_m]^{\text{T}}$ and the charges are given by $\boldsymbol{q} = [q_1, q_2, ...q_m]^{\text{T}}$, the relationship between the two is

$$\boldsymbol{V} = [C]^{-1}\boldsymbol{q} \tag{2}$$

where $[C]$ is the Position Dependent Capacitance (PDC) matrix whose inverse is defined below:[11]

$$\boldsymbol{V} = [C]^{-1}\boldsymbol{q} = \frac{1}{4\pi\epsilon_0}\begin{bmatrix} 1/R_1 & 1/\rho_{1,2} & \cdots & 1/\rho_{1,m} \\ 1/\rho_{2,1} & 1/R_2 & \cdots & 1/\rho_{2,m} \\ \vdots & \vdots & \ddots & \vdots \\ 1/\rho_{m,1} & 1/\rho_{m,2} & \cdots & 1/R_m \end{bmatrix}\begin{bmatrix} q_1 \\ q_2 \\ \vdots \\ q_m \end{bmatrix} \tag{3}$$

The voltage on each sphere can be determined as a function of various factors, such as photoelectron current resulting from UV radiation and interactions with the plasma environment.[1,4] For purposes of this paper, the charged bodies are assumed to be perfect conductors. Thus, the voltage of each sphere for a given body is the same ($V_i = V_j$) and is equal to the voltage of the body. The PDC matrix can be inverted to obtain the charge on each sphere. Once the charges on each sphere are known, the forces and torques can be computed as shown in Eqs. (4) and (5). An origin O at the

3

center of mass of the body is used for $\boldsymbol{r}_i$; the force and torque calculated about this origin are

$$\boldsymbol{F} = -k_c q_B \sum_{i=1}^{n} \frac{q_i}{r_{i,b}{}^3} \boldsymbol{r}_{i,b} \tag{4}$$

$$\boldsymbol{L}_O = -k_c q_B \sum_{i=1}^{n} \frac{q_i}{r_{i,b}{}^3} \boldsymbol{r}_i \times \boldsymbol{r}_{i,b} \tag{5}$$

With minimal loss of accuracy — of a few percent or less — MSM is a promising way to solve for the electrostatic forces and torque on a spacecraft faster than real-time. However, it relies on knowledge of the position and size of all spheres in the model, which in previous work have been laboriously hand tuned.[11, 12] This paper seeks to develop an automated means of determining the position and size of these spheres, such that the force and torque calculated from the model match closely with the data provided by a commercial electrostatic FEA tool.

MSM Capacitance Matrix Invertibility

The inverse of the PDC matrix is easily formed, but must be inverted to solve for the charges, which are needed to compute the force and torque. Certain combinations of MSM parameters can make this inversion difficult or even impossible. Degenerate matrices produced by these parameters yield non-physical results, such as negative self capacitance.

One way to ensure the invertibility of a matrix is to make sure the determinant is non-zero. This can be done analytically for some simple cases and yields relationships between MSM model parameters that must be avoided to ensure the validity of the model. For general cases with a large number of spheres, the condition number of the inverse of the PDC matrix may be used to measure how close the given MSM parameters are to causing a singularity. Parameter sets that yield high condition numbers should be avoided. The issue of how best to address such ill-conditioning of particular MSM parameters remains an open research question. For the scope of this paper, this issue is identified and initial MSM parameters are selected for the numerical optimizations that are removed from such singular configurations.

SELF CAPACITANCE CONSIDERATIONS

MSM Self Capacitance Definition

The force acting on two charged objects is due to the interaction of the charges on the first object with the strong electric field created by the charges on the second. If the voltage is known, the key to predicting the forces and torques acting upon an object is determining the charge. This is done using the relationship between charge and voltage known as self capacitance as seen in Eq. (6). For an individual sphere there is an analytic form for the self capacitance ($C = 4\pi\epsilon_0 r$). In the general case, a body modeled by MSM, has a self capacitance based on the sphere geometry. The self capacitance is the ratio of the total charge Q on the object to its surface voltage V

$$C = \frac{Q}{V} \tag{6}$$

The total charge is given by

$$Q = \sum_{i=1}^{N} q_i \tag{7}$$

4

Using Eq. (6) the charge vector is written as

$$q_i = \sum_{j=1}^{N} C_{ij} V_j \tag{8}$$

Recalling that the voltage on each sphere within the object is assumed to be the same ($V_j = V$), substituting Eqs. (7) and (8) into Eq. (6) yields

$$C = \frac{Q}{V} = \frac{\sum_{i=1}^{N} \sum_{j=1}^{N} C_{ij} V_j}{V} = \sum_{i=1}^{N} \sum_{j=1}^{N} C_{ij} \tag{9}$$

The total capacitance C of an MSM model is the sum of the individual elements of the PDC matrix $[C]$. Recall that $[C]$ is obtained by inverting $[C]^{-1}$, defined in Eq. (3).

Self Capacitance Optimization Constraint

Previous work with MSM focused on matching forces and torques between two charged objects separated by less than ten craft radii without regard to matching the self capacitance of the objects.[11] An MSM geometry determined under these conditions will generally perform well at these distances, but will suffer from significant errors at larger distances. As the separation distance between the two objects grows large, the objects will effectively become as isolated point spheres. At this point, the total charge of each object is approximated with Eq. (6), which only requires knowledge of the self-capacitance. If the MSM parameters do not yield a self-capacitance C which matches the self-capacitance of the actual shape, then the electrostatic force predictions are ensured to be incorrect at large separation distances.

The proposed MSM optimization method constrains the self capacitance calculated using Eq. (9) to be equal to the self capacitance found using an commercial electrostatic FEA tool. The three primary benefits for using this constraint are:

- The MSM solution will automatically provide accurate results at large distances.

   By enforcing fundamental physics, predicting forces in the far field will always give good results, while still allowing the subtlety needed to model the complex interactions in the near field.

- The MSM optimization will no longer be swayed by noisy data in the far field.

   Generating or measuring truth forces and torques becomes increasingly noisy as the separation distance between charged objects increases. Fitting the MSM parameters to match such noisy data can pose significant challenges to numerical optimization algorithms and can reduce the accuracy of the solution. Instead, by constraining the MSM parameters to satisfy the known self-capacitance of a shape, the lower quality electrostatic force and torque solutions at larger separation distances can be ignored.

- Enforcing the self capacitance constraint eliminates one degree of freedom.

   By reducing the MSM parameter search space, the computational time for the optimization process is reduced. It goes without saying that this is desirable in the automation of sphere geometry. However, this reduced computational time can come at the cost of slightly decreased accuracy in cases where separation distances is small.

The self capacitance constraint can be enforced either numerically or analytically. An analytical constraint is always more accurate than a numerical constraint. However, an analytical constraint may not always be available. Forming the self capacitance requires inverting an $N \times N$ matrix and summing all the elements, where N is the number of spheres in the MSM model. This can become difficult for cases involving a large number of spheres.

MODEL PARAMETER OPTIMIZATION

An optimal MSM sphere distribution can be obtained by employing optimization techniques, whereby the desired sphere distribution minimizes the force and torque prediction error. Optimizing the sphere distribution uses the size and body-fixed location of each MSM sphere included in the model as state variables. For this analysis, MATLAB's built-in *fmincon* optimizer is used.

Cost Functions

Optimization problems are driven by a cost function. Two cost functions were implemented and compared in this study. The first cost function J_{rel}, based on the relative difference between VMSM and Maxwell forces and torques, is defined as:

$$J_{\text{rel}} = f_{\text{rel}} + t_{\text{rel}} \tag{10}$$

$$f_{\text{rel}} = \sum_{i=1}^{n} \frac{||\boldsymbol{F}_{\text{VMSM}_i} - \boldsymbol{F}_{\text{Maxwell}_i}||}{||\boldsymbol{F}_{\text{Maxwell}_i}||} \tag{11}$$

$$t_{\text{rel}} = \sum_{i=1}^{n} \frac{||\boldsymbol{T}_{\text{VMSM}_i} - \boldsymbol{T}_{\text{Maxwell}_i}||}{||\boldsymbol{T}_{\text{Maxwell}_i}||} \tag{12}$$

Where $\boldsymbol{F}_{\text{MSM}_i}$ denotes the predicted force vector at the ith comparison point, $\boldsymbol{F}_{\text{Maxwell}_i}$ is the truth model force vector evaluated at that same comparison point, and similar definitions are made for torque. One drawback of using relative differences in a cost function is the potential for small absolute differences to result in large relative differences. This is very likely to happen in the far field when the force and torque in the truth model are very small.

Consequently, the second cost function J_{abs} is based on the absolute difference between VMSM and Maxwell forces and torques:

$$J_{\text{abs}} = f_{\text{abs}} + t_{\text{abs}} \tag{13}$$

$$f_{\text{abs}} = \frac{\sum\limits_{i=1}^{n} ||\boldsymbol{F}_{\text{VMSM}_i} - \boldsymbol{F}_{\text{Maxwell}_i}||}{\sum\limits_{i=1}^{n} ||\boldsymbol{F}_{\text{Maxwell}_i}||} \tag{14}$$

$$t_{\text{abs}} = \frac{\sum\limits_{i=1}^{n} ||\boldsymbol{T}_{\text{VMSM}_i} - \boldsymbol{T}_{\text{Maxwell}_i}||}{\sum\limits_{i=1}^{n} ||\boldsymbol{T}_{\text{Maxwell}_i}||} \tag{15}$$

By distributing the sum into the denominator, errors that occur when the FEA solution is small are not heavily weighted. This is advantageous because when the FEA force and torque are small, there is often a lot of noise in the solution.

6

To easily assess the quality of the solution, Eqs. (11) and (12), which are analogous to relative error, can be used. Since f_{rel} and t_{rel} are cumulative quantities, their averages will provide a relative error representative of the quality of a given solution. This relative error can be multiplied by 100 to obtain a percentage error measure that is used to quantify the quality of a particular geometric solution determined by optimization during this analysis.

PROTOTYPE CHARGED SPACE OBJECT

A convenient system to model is a cylinder, representing a defunct rocket body upper stage, and a sphere, representing a controlled and charged space tug. The cylinder has a length of three meters and a diameter of one meter, and the sphere has a diameter of one meter. In Reference 11 the cylinder is approximated using three collinear spheres, as shown in Figure 5, with the end spheres set at an equal distance away from the center sphere. The cylinder models with either two or three collinear spheres are considered in the scope of this paper.

Electrostatic Force Truth Model

The commercial electrostatic FEA tool Maxwell 3D is used to calculate the forces and torques between the cylinder and the sphere. Both the cylinder and the sphere are held at +30,000 Volts. Forces and torques are calculated at multiple points as shown in Figure 3. The points are distributed cylindrically, with radius changing by one meter and angle changing by 15° between each point. These points can be grouped by their distance from the cylinder; each set of equidistant points is referred to as a *ring* and are labeled in Figure 3.

The points included in the rings at larger distances will have smaller forces that are either negligible or describable by approximating the cylinder with a single sphere. It may be unnecessary to include these rings in the optimization process, particularly if solution quality is not reduced. Thus, this analysis will also examine the effects of these rings on solution quality and computational time.
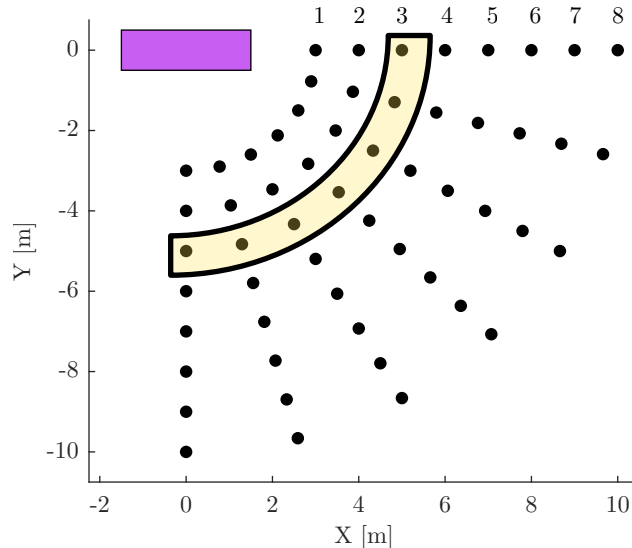
Figure 3. Geometric Parameters for Maxwell Force and Torque Calculations
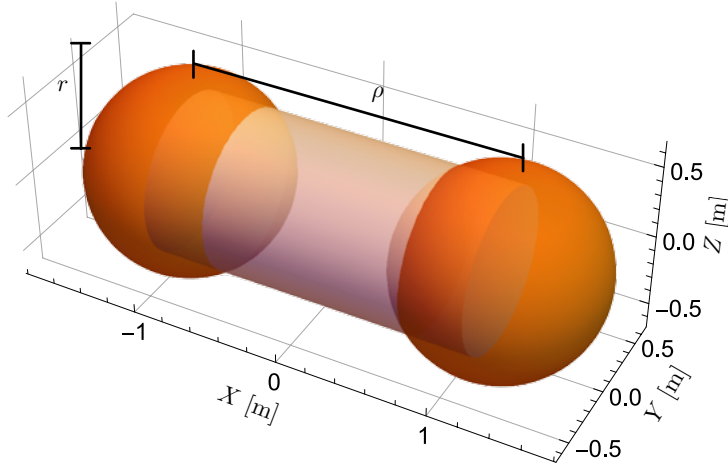
Figure 4. Two Sphere MSM Model of a Cylinder

Self Capacitance Matching

2-Sphere MSM Self Capacitance Consider a cylinder modeled by 2 collinear spheres of equal radius, as shown in Figure 4. The model is described by two independent variables: the radii of each sphere r and the distance between the two spheres ρ.

Eq. (9) is used to express the self capacitance of the two sphere system as

$$C = 4\pi\epsilon_0 \frac{2r\rho}{\rho + r} \tag{16}$$

The independent variables r and ρ are expressed individually as

$$r = \frac{\rho C_{\text{mod}}}{2\rho - C_{\text{mod}}} \tag{17}$$

$$\rho = \frac{r C_{\text{mod}}}{2r - C_{\text{mod}}} \tag{18}$$

where C_{mod} is the scaled self capacitance

$$C_{\text{mod}} = \frac{C}{4\pi\epsilon_o} \tag{19}$$

Eq. (17) is used to write r as a function of ρ or vice versa with Eq. (18). Thus, there is only one independent variable in this two sphere MSM case.

3-Sphere MSM Self Capacitance Next, a cylinder is modeled by 3 collinear spheres, as shown in Figure 5. In this case, the identically sized end spheres are equidistant from the center sphere, which has a different radius. Three independent variables exist in this scenario: the radii of the end sphere r, the radius of the center sphere R, and the distance between the center sphere and the end sphere ρ.

As with the 2 sphere model, there are analytic results for the self capacitance of the sphere in terms of the axially constrained MSM sphere placement and size parameters. The self capacitance is

$$C = 4\pi\epsilon_0 \frac{\rho(-7rR + 2\rho(2r + R))}{\rho(2\rho + r) - 4rR} \tag{20}$$

8
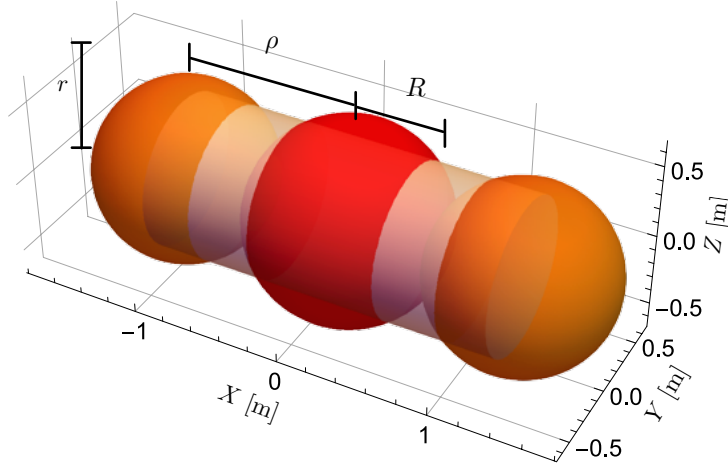
Figure 5. Three Sphere MSM Model of a Cylinder

Direct substitution yields a reduced set of unknown MSM parameters and allows the 3 MSM parameters to be expressed in terms of the other 2 and the true self capacitance using:

$$r = \frac{2\rho^2(R - C_{\text{mod}})}{C_{\text{mod}}\rho - 4C_{\text{mod}}R + 7R\rho - 4\rho^2} \tag{21}$$

$$R = \frac{\rho(4r - 2C_{\text{mod}}\rho - C_{\text{mod}}r)}{7r\rho - 2\rho^2 - 4C_{\text{mod}}r} \tag{22}$$

$$\rho = \frac{-(C_{\text{mod}}r + 7rR) \pm \sqrt{(C_{\text{mod}}r + 7rR)^2 + 4(2C_{\text{mod}} - 4r + 2R)(4C_{\text{mod}}Rr)}}{2(2C_{\text{mod}} - 4r + 2R)} \tag{23}$$

This allows the numerical optimizer to search only 2 parameters instead of the original 3. If only the set of three parameters (R, r, ρ) are considered that satisfy the MSM self capacitance equality constraint, all admissable MSM parameters must lie on a two-dimensional surface, as shown in Figure 6.

Although analytical constraints exist for the restricted 2-sphere and 3-sphere MSM cases, such a simple solution may not always exist. In the general case of N spheres, a numerical constraint must be enforced.

Matrix Inversion

As noted in the Matrix Invertibility section, certain sets of MSM parameters can make the inverse of the PDC difficult or impossible to invert, which yields non-physical results such as negative or infinite self capacitance. To avoid these singularities, the determinant can be analytically constrained to be non-zero, which yields relationships between MSM parameters to be avoided. This is done for the 2- and 3-sphere cases considered in this paper.

2-Sphere Case   For two collinear spheres of equal radius, the inverse of the PDC is given by

$$[C]^{-1} = \frac{1}{4\pi\epsilon_0} \begin{bmatrix} \dfrac{1}{R} & \dfrac{1}{\rho} \\ \dfrac{1}{\rho} & \dfrac{1}{R} \end{bmatrix} \tag{24}$$
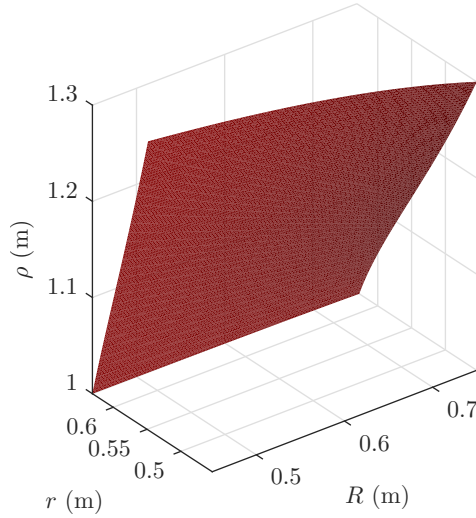
Figure 6. Isosurface Showing Where the Cylinder Self-Capacitance is 106.8345 pF

Where R is the sphere radius and ρ is their separation. The determinant of this matrix is

$$\det([C]) = \frac{1}{R^2} - \frac{1}{\rho^2}$$

By ensuring $R \neq \rho$ the matrix is invertible and MSM provides valid results. In addition, as $R \to \rho$ the matrix becomes numerically ill-conditioned.

3-Sphere Case For three collinear spheres, where the outer spheres are constrained to be the same size but the center sphere radius is free, the matrix is somewhat more complicated. The inverse of the capacitance matrix is now given by

$$[C]^{-1} = \frac{1}{4\pi\epsilon_0} \begin{bmatrix} \dfrac{1}{r} & \dfrac{1}{\rho} & \dfrac{1}{2\rho} \\ \dfrac{1}{\rho} & \dfrac{1}{R} & \dfrac{1}{\rho} \\ \dfrac{1}{2\rho} & \dfrac{1}{\rho} & \dfrac{1}{r} \end{bmatrix} \tag{25}$$

Where r is the end sphere radius, R is the center sphere radius, and ρ is the distance from the center of the end sphere to the center of the center sphere. The determinant is now

$$\det([C]) = \frac{(2\rho - r)(2\rho^2 + r\rho - 4rR)}{4\rho^3 r^2 R} \tag{26}$$

This determinant has two roots: $2\rho - r = 0$ and $2\rho^2 + r\rho - 4rR = 0$. The first one is easily visualized as the end radius being twice the distance to the center. This means that the edge of the leftmost sphere touches the center of the rightmost sphere. The parameter sets of both roots are illustrated in Figure 7.

These surfaces in the 3-dimensional parameter space must be avoided to ensure model validity. This does not reduce the degrees of freedom, but does require parameter checking.

10
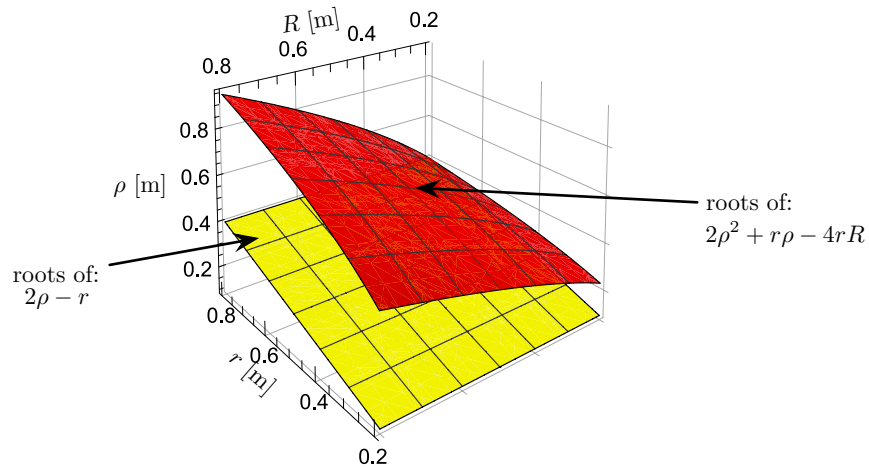
Figure 7. Surfaces where the determinant of the PDC Matrix is zero

OPTIMIZATION CASES

The goal of this study is to automate the process of distributing MSM spheres through the volume of a body to best match the force and torque experienced by that body when in the presence of a second craft. The automation process uses an optimization routine to move the center position and set the radius of each MSM sphere. The optimization state therefore becomes the set of geometrical parameters that describe the locations and sizes of all MSM spheres in the body. The baseline to which new geometric parameters are compared are the numbers in Table 1, which are presented in Reference 11. The coordinates and sphere definitions in Table 1 are based on the geometry of Figure 5.

Table 1. Baseline Geometric Parameters

	Sphere 1	Sphere 2	Sphere 3
X Coordinate (m)	0	0	0
Y Coordinate (m)	-1.1454	0	1.1454
Z Coordinate (m)	0	0	0
Radius (m)	0.5959	0.6534	0.5959

The baseline geometric parameters can be expressed in the three parameter set as

$$R = 0.6534$$
$$r = 0.5959$$
$$\rho = 1.1454$$

These parameters generate a solution with a relative force error of 1.47% and a relative torque error of 1.18%.

The initial conditions for the optimization create spheres of equal radii that have surface area equal to the cylinder model. Under these conditions, the optimization produces solutions with

11

relative errors ranging from 1.1% to 3.9% for force and 0.1% to 4.1% for torque, depending on the number of data-point rings used in the optimization, the inclusion of the capacitance constraint, and the cost function used. Generally speaking, the solutions provided by this optimizer approach are comparable to the accuracy previously achieved with the significant benefit that all solutions are generated in less than ten seconds — orders of magnitude faster than the thousands of seconds previously required.[12]

Four cases are examined in further detail to demonstrate the flexibility of the algorithm and the current challenges in automating sphere placement: a three sphere cylinder model with and without the previously described capacitance constraint and a two sphere cylinder model with and without the previously described capacitance constraint. Each case is analyzed with the relative and absolute difference cost functions, as described by Eqs. (10) and (13). The best results of all eight cases are tabulated in Table 2.

3-Sphere, 3 MSM Parameters Model

The first case uses three spheres to model the cylinder and does not use a capacitance constraint, as shown in Figure 5. The initial conditions chosen for the optimization are $r = R = 0.54$ meters and $\rho = 1.5$ meters.

Figure 8 plots the relative force and torque error and computational time against the number of rings used in the optimization. It should be noted that, even if less than eight rings were used for the optimization, the relative error is calculated by comparing the solution against all possible data points in the eight rings. As expected, including more data in the optimization improves the prediction over the data range considered. An important aspect of this trend is how both the force and torque error begin to level out when more than three rings are included. This indicates that data from outer rings could be ignored, especially since computational times increase with increased data.

The relative difference and absolute difference cost functions complete the optimization in about the same about of time. However, the relative difference cost function shows significantly lower error in force and torque as the number of rings used in the optimization increases. Particularly notable is the near-zero torque error when seven or eight rings of data are used. Because of this, it can be concluded that the relative difference cost function is much better at matching data than the absolute difference cost function.

3-Sphere, 2 MSM Parameters Model

The second case uses the same three sphere setup as the first, but adds an analytical capacitance constraint as described by Eqs. (21) through (23). In this case, the constraint for the end radius r, is implemented, leaving the center radius R and the separation distance ρ as the independent variables.

In Figure 9, the relative force and torque error and computational time are plotted against the number of rings used in the optimization. Of note of the error trends under the capacitance constraint is the force error, which remains constant regardless of the number of rings used. This is due to the nature of the capacitance constraint, which causes the VMSM model to resemble a single point charge at large distances. At large distances, all that is needed to model force is the capacitance of the object.[12] While matching capacitance can model force with a high degree of accuracy, it cannot model torque quite as well because of induced charging effects on the cylinder.

(a) Relative Difference Cost Function   (b) Absolute Difference Cost Function
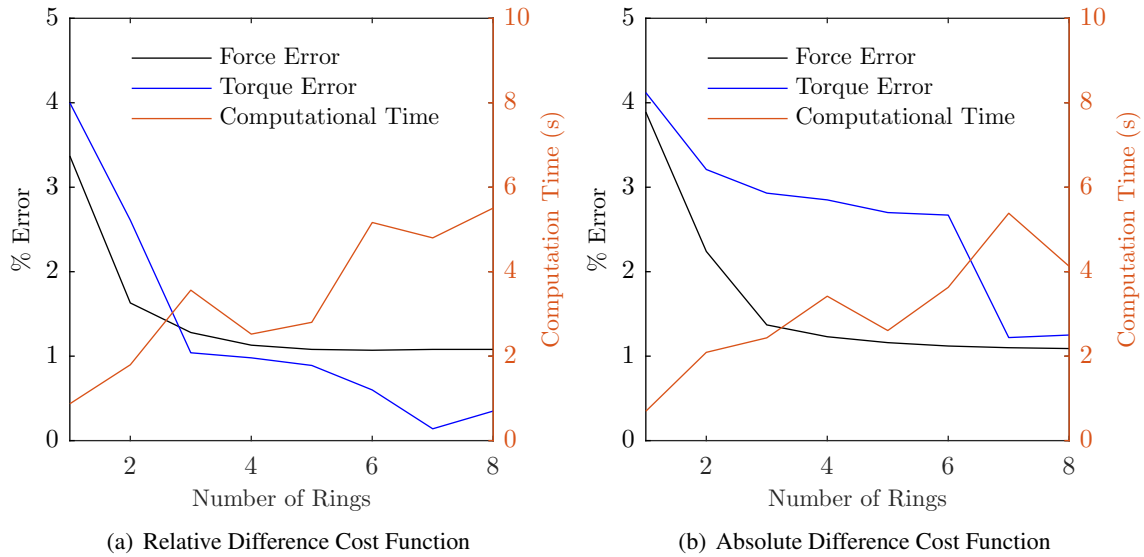
Figure 8. Three Sphere VMSM Performance, Without Capacitance Constraint

With the exception of using seven or eight rings under the absolute difference cost function, the 2 Parameter Model completes the optimization more quickly than the 3 Parameter Model. This supports the assumption that reducing the parameter search space would decrease the computation time. Since both the 3 Parameter Model and 2 Parameter Model result in similar errors, it may be more useful to use the 2 Parameter Model for optimizations on account of its speed.

2-Sphere 2 MSM Parameters Model

The third case uses a two sphere model for the cylinder, as shown in Figure 4, without the capacitance constraint. The initial conditions chosen are $r = 0.6614$ meters and $\rho = 1.5$ meters. Because there are only two independent variables (r and ρ), the optimization in this case should run much faster than that for the unconstrained three sphere model. This is observed in Figure 10, where computational time for determining the solution is under two seconds for most ring and cost function combinations. In contrast, many of the three sphere cases, even if constrained by capacitance to use two parameters, took more than three seconds to find a solution.

As with the three sphere models, the errors on the two sphere model, particularly for force, begin to level off after three rings of data are used; this is especially apparent for the absolute difference cost function. This trend indicates that not all rings are necessary to produce a solution that can reasonably match a truth model. The relative difference cost function also provides lower errors in torque than the absolute difference cost function, suggesting again that the relative difference cost function is better suited for these optimizations.

The errors in the two sphere model are on the same order of magnitude as for the three sphere model, while the optimization takes about half the time to run. This suggests that it may be more practical to use the two sphere model in some cases, particularly where computational time is of importance.

13

(a) Relative Difference Cost Function　　　(b) Absolute Difference Cost Function
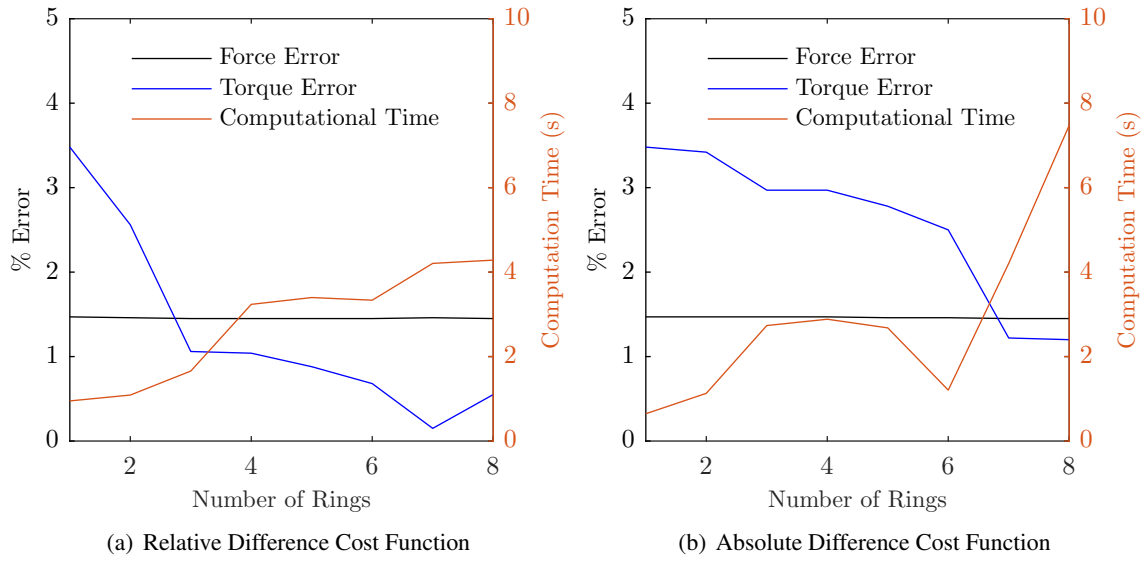
Figure 9. Three Sphere VMSM Performance, With Capacitance Constraint

(a) Relative Difference Cost Function　　　(b) Absolute Difference Cost Function
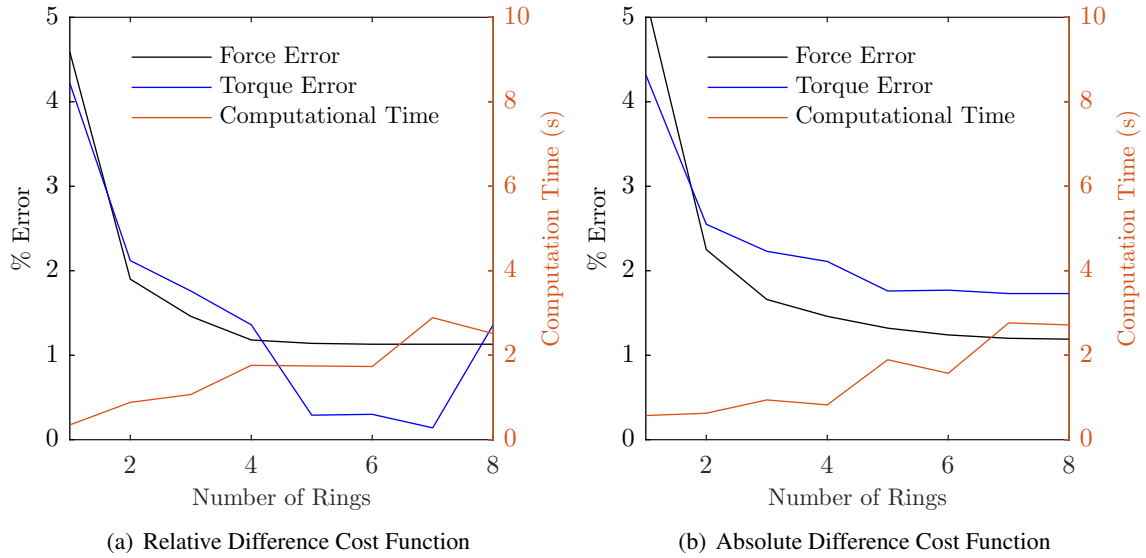
Figure 10. Two Sphere VMSM Performance, Without Capacitance Constraint

14

2-Sphere 1 MSM Parameter Model

The fourth case uses a two sphere model for the cylinder while enforcing a capacitance constraint. By using Eq. (23) to constrain the optimization to one independent variable r, the computational time should decrease while having minimal effects on the errors. Figure 11 shows the error and computational time plots.

As with the capacitance constrained three sphere model (Figure 9), the force errors in this case are constant regardless of the number of rings used for the optimization. While it was expected that the capacitance constraint would allow force to be accurately accounted for at large distance, the constant errors provided by the solution were not. It appears that the capacitance of the model, rather than the geometric sphere configuration, is key to accurately determining forces acting on a charged object.

While capacitance cannot provide the same accuracy for torque calculations, it is still notable that errors change very little after five rings of data are included — even dropping below 1% error. It should be noted that such low error values may very well result from overfitting a solution to noisy data; however, the low errors demonstrate that it is possible to obtain close matches to truth data without using all the rings available.

(a) Relative Difference Cost Function   (b) Absolute Difference Cost Function
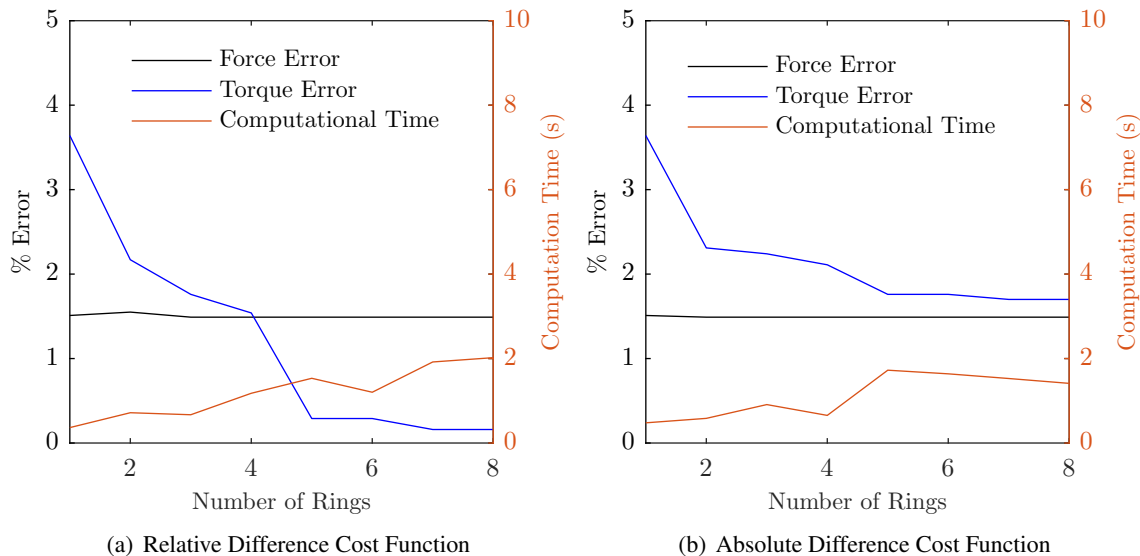
Figure 11. Two Sphere VMSM Performance, With Capacitance Constraint

2-Sphere Cost Functions

It is useful to visualize the cost functions to understand why the optimization may have chosen a given solution and why computational times seem to differ between functions. Because it is difficult to visualize cost functions of three parameters, only the functions for the two sphere models are analyzed.

The cost surface for the two sphere VMSM can be visualized as shown in Figure 12, where the darker hues indicates a lower — and thus more desirable — cost. The black line on the plot indicates the successive steps that the optimization under the relative difference cost function follows. In

(a) Without Capacitance Constraint (b) With Capacitance Constraint
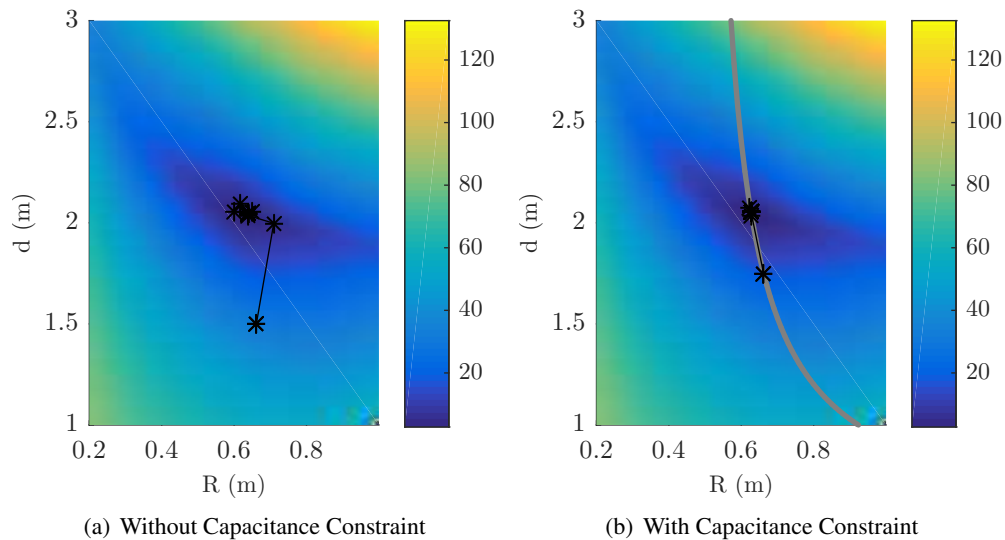
Figure 12. Two Sphere Model Cost Surfaces

Figure 12(b), a gray line is plotted to indicate the space of all points that satisfy the capacitance constraint.

An important aspect of the cost surface is the gradient around the minima where the solution converges. Although it is somewhat difficult to identify with the provided visualization, the gradient around that minima is smaller than at other points on the surface. This can make convergence on a solution difficult, which may explain why errors sometimes increase after including more rings.

Figure 12(b) illustrates one of the strengths of using the capacitance constraint: fast convergence on a solution. Because the search space has only one degree of freedom, it finds the local minima very quickly. Only one point, the initial condition, lies outside the minima where the optimized solution is found. It is not coincidental that the optimizer converged on a solution for this constrained case more quickly than any other case analyzed. Due to the capacitance constraint, the optimizer need only find the local minima on the capacitance line, rather than on an entire plane. A similar scenario likely exists when constraining the search space for the three sphere from a volume to a plane.

Summary of Cases

Table 2 lists the best fit each cost function achieved in addition to the fit from the baseline geometric parameters. The most noticeable aspect of these numbers is the computational time of the optimization — three orders of magnitude faster than what had previously been achieved. This increased speed does not seem to have much cost associated with it, as errors are equivalent to or better than the baseline parameters. Even faster computational times, typically about half of the values listed here, can be achieved at an increase to the force and torque errors. This speed increase in determining suitable MSM parameters is particularly promising for future work that will consider larger numbers of MSM spheres or allow spheres to be generally distributed about the object geometry. Both scenarios will involve a larger number of MSM parameters which is more taxing on the setup optimization process.

16

Table 2. Comparison of Optimized Parameters

Cost Function	Force Error (%)	Torque Error (%)	Computational Time (sec)	Number of Rings Used
3 Sphere 3 Param. Abs. Difference	1.10	1.22	5.38	7
3 Sphere 3 Param. Rel. Difference	1.08	0.14	4.80	7
3 Sphere 2 Param. Abs. Difference	1.45	1.22	4.21	7
3 Sphere 2 Param. Rel. Difference	1.46	0.15	4.21	7
2 Sphere 2 Param. Abs. Difference	1.19	1.73	2.72	8
2 Sphere 2 Param. Rel. Difference	1.13	0.14	2.89	7
2 Sphere 1 Param. Abs. Difference	1.49	1.70	1.41	8
2 Sphere 1 Param. Rel. Difference	1.49	0.16	1.92	7
Baseline Geometric Parameters	1.47	1.18	4443.1[12]	N/A

These results show that automated geometry optimization is indeed possible using the VMSM. It should be noted that cost functions that generate very small errors should not be assumed to be the best function. Recall that the truth model is based on a commercial electrostatic FEA tool, which is subject to numerical error. Additionally, the percentage errors of even the worst fits do not go beyond 4%; in actual scenarios involving electrostatic charging, uncertainties in the environment may very well be larger than any inaccuracies introduced by these optimizations. Consequently, the determination of the "best" cost function should weigh other factors, with computational time being the most likely.

There is a noticeable decrease in torque error when using the relative difference cost function when compared to the absolute difference cost function. While the exact reasons for this trend are as yet unclear, it is an important consideration because it can provide more accurate results with minimal increase in computation time.

In comparing computational time, there is a marked advantage when using the capacitance constraint, as it reduces the search space by an entire DOF. In addition the speeding up computation, the capacitance constraint implies accurate force prediction at larger distances due to the inverse square law reducing distant objects to single point charges. While the torque solution may be slightly less accurate due to the lost DOF, the overall errors are still not very large, particularly when considering the uncertainties inherent in space missions.

CONCLUSION

The methods of optimizing MSM sphere placement presented here show that it is possible to automate the geometry optimization for the VMSM and quickly obtain accurate results. The relative difference cost function provides lower errors than the absolute difference cost function, with similar performance in force error and computational time. Constraining the optimization so that it matches capacitance significantly reduces the computational time and provides the added benefit of predicting forces more accurately between distant objects. Computational time can also be reduced by removing distant data points from consideration in the optimization, with minimal effect on accuracy.

The VMSM models applied here achieve accuracy comparable to baseline parameters for simple

cylinders and when the line of the cylinder is known. Future work will investigate automated optimization for more complex shapes and instances where the plane or line of the object may not be known. It is possible that other configurations of spheres, such as non-collinear spheres or more than three spheres, could create a more optimal solution depending on the constraints and configurations used, thus further increasing the DOF that must be optimized.

ACKNOWLEDGMENT

REFERENCES

[1] S. T. Lai, *Fundamentals of Spacecraft Charging*. Princeton University Press, 2012.

[2] R. G. Johnson, R. Strangeway, S. Kaye, R. Sharp, and E. Shelley, "SCATHA Observations of Space Plasma Composition During a Spacecraft Charging Event," tech. rep., Lockheed Palo Alto Research Laboratory, 1979.

[3] E. A. Hogan and H. Schaub, "General High-Altitude Orbit Corrections Using Electrostatic Tugging with Charge Control," *Jounral of Guidance, Control, and Dynamics*, Vol. 38, April 2015, pp. 699–705.

[4] H. Schaub and Z. Sternovsky, "Active Space Debris Charging for Contactless Electrostatic Disposal Maneuvers," *Advances in Space Research*, Vol. 53, No. 1, 2014, pp. 110–118.

[5] T. Bennett, D. Stevenson, E. Hogan, and H. Schaub, "Prospects and Challenges of Touchless Electrostatic Detumbling of Small Bodies," *Advances in Space Research*, Vol. 56, August 2015, pp. 557–568.

[6] E. A. Hogan and H. Schaub, "Impacts of Tug and Debris Sizes on Electrostatic Tractor Charging Performance," *Advances in Space Research*, Vol. 55, January 2015, pp. 630–638.

[7] H. Schaub and D. F. Moorer, "Geosynchronous Large Debris Reorbiter: Challenges and Prospects," *AAS/AIAA Kyle T. Alfriend Astrodynamics Symposium*, May 17-19 2010.

[8] B. Streetman and M. A. Peck, "New Synchronous Orbit Using the Geomagnetic Lorentz Force," *Journal of Guidance, Control, and Dynamics*, Vol. 30, November-December 2007, pp. 1677–1689.

[9] B. Streetman and M. A. Peck, "General Bang-Bang Control Method for Lorentz Augmented Orbits," *Journal of Spacecraft and Rockets*, Vol. 47, May-June 2010, pp. 484–492.

[10] B. Streetman and M. A. Peck, "Gravity-Assist Maneuvers Augmented by the Lorentz Force," *Journal of Guidance, Control, and Dynamics*, Vol. 32, September-October 2009, pp. 1639–1647.

[11] D. Stevenson and H. Schaub, "Multi-Sphere Method for Modeling Spacecraft Electrostatic Forces and Torques," *Advances in Space Research*, Vol. 51, Jan 2013, pp. 10–20.

[12] D. Stevenson and H. Schaub, "Optimization of Sphere Population for Electrostatic Multi-Sphere Method," *IEEE Transactions on Plasma Science*, Vol. 41, December 2013.